

Controlling cooperative emission and superradiance in waveguide-coupled quantum dots

D. Hallett,^{1,*} J. Wiercinski,^{2,†} L. Hallacy,¹ S. Sheldon,¹ R. Dost,¹ N. Martin,¹ A. Fenzl,¹ I. Farrer,³ A. Verma,³ M. Cygorek,⁴ E. M. Gauger,² M. S. Skolnick,¹ and L. R. Wilson¹

¹*Department of Physics and Astronomy, University of Sheffield, Sheffield, S3 7RH, UK*

²*SUPA, Institute of Photonics and Quantum Sciences,*

Heriot-Watt University, Edinburgh EH14 4AS, United Kingdom

³*Department of Electronic and Electrical Engineering, University of Sheffield, Sheffield, S1 3JD, UK*

⁴*Condensed Matter Theory, Department of Physics, TU Dortmund, 44227 Dortmund, Germany*

(Dated: October 24, 2024)

We report the measurement of collective emission from a pair of independently tuneable InAs quantum dots embedded in a nanophotonic waveguide. A split diode structure allows independent electrical control of the quantum dot transition energies over a wide range with minimal loss in waveguide coupling efficiency. We utilise this to systematically map out the transition from collective to independent emission. We perform both lifetime as well as Hanbury Brown-Twiss measurements on the device, observing anti-dips in the photon coincidences indicating collective emission while at the same time observing a drop in lifetime around zero detuning, indicating superradiant behaviour. Performing both measurement types allows us to investigate detuning regions which show both superradiant rate enhancement and inter-emitter coherence, as well as regions in which correlations persist in the absence of rate enhancement.

I. INTRODUCTION

Coherent interactions between quantum emitters are vital for the scaling up of many quantum information schemes [1, 2]. Multiple indistinguishable quantum emitters can couple to an optical mode as a single entity [3], experiencing enhanced light-matter coupling [4] and creating strongly correlated emission [5]. Optical coupling between multiple quantum emitters enables the generation of light with non-classical photon statistics [6–8] entanglement between qubits [9–12], and advanced quantum photonic circuits [13, 14]. Moreover, quantum enhancement of the light-matter interaction is the basis for superabsorbers for light harvesting and quantum batteries [15], while the concomitant effect of subradiance can protect quantum memories against losses [16, 17], and enable long-range exciton transfer [18, 19].

These applications motivate current efforts to demonstrate and control superradiance in solid-state quantum devices. Self-assembled quantum dots (QDs) have emerged as a leading platform by combining the practicality of handling solid-state emitters at fixed positions with the excellent optical properties of self-assembled QDs [20, 21], and the near-unity beta factor of nanophotonic waveguides [22, 23]. Moreover, it has been shown that phonon effects, often a limiting property of solid-state emitters, are not necessarily a major obstacle for long-time inter-emitter entanglement in solid-state devices at low temperatures [24, 25].

Nevertheless there are several challenges to overcome in order to scale up superradiant solid-state quantum devices: First, QDs typically grow with random sizes and geometries, which means that some way of tuning different QDs into resonance is required to achieve spectral indistinguishability of the QDs. Relative tuning of QD energies can be achieved through control of temperature [26], strain [27], magnetic field [28] or electric field [29]. However these tuning methods can be slow, irreversible or unsuited for scale-up. Second, superradiance requires spatial indistinguishability of the quantum emitters. In free space this is achieved by confining the emitters to small volumes such that the distances between emitters is smaller than the wavelength of the light. However, the typical density of QDs is such that QDs of comparable energies are spatially separated farther than the wavelength of the emitted light, especially because the latter is shortened by the larger refractive index in typical semiconductor materials [29]. An attractive solution to achieve superradiance between spatially separate solid state emitters is therefore to coherently couple them to a photonic structure such as a waveguide [26, 27], where the confinement of waveguide modes in one dimension enables collective coupling to the electromagnetic field over long distances. Such a system can also allow observation of a long-lived subradiant state [28].

Previous theoretical work has shown that superradiant ensembles also show a characteristic anti-dip in photon coincidences measured in an Hanbury Brown-Twiss (HBT) setup [30]. Based on this, existing experimental work on superradiance in solid-state emitters has used either the change in decay rate and the presence of a dark state [28], or photon coincidence

* d.hallett@sheffield.ac.uk

† jehw2000@hw.ac.uk

measurements [26, 27, 31] to demonstrate the presence of superradiance. For this, mostly the case of zero detuning has been compared to a far detuned case, in which the emitters are assumed to behave independently. However, quantitative changes in the photon emission rate may have origins different from superradiance, e.g., variations of the dipole of a single emitter resulting from changes of the wave function upon tuning, or contributions from dark exciton states [22]. An anti-dip observed in HBT experiments could in principle be used to indicate the presence of coherence between the QDs at resonance. However, a similar signature has also been seen in a setup of two resonant QDs where the spatial separation was too large to sustain superradiance [29]. There, the anti-dip was caused by measurement-induced entanglement due to the erasure of which-path information about which QD emitted the first photon. Therefore, it is desirable to measure *both* photon coincidences as well as changes in the lifetime, while *continuously varying* the detuning between the QDs to demonstrate the presence of superradiance.

Here, we demonstrate measurements of both lifetimes and photon coincidences, on two independently tuneable QDs coupled to a nanobeam waveguide. Independent tuning of the QDs is achieved by separate electrical gating [32]. This gating method allows fast, repeatable tuning of individual emitters, without compromising transmission through the photonic device, while at the same time being scalable to larger QD numbers. Optical gating of one QD [33, 34] is used to switch between—and therefore directly compare—superradiant and non-superradiant regimes, by effectively adding and removing one emitter. Measurements of the decay rate of the system indicate a clear enhancement of the decay rate when the emitters are resonant. Additionally, we confirm the presence of strong QD-QD correlations by performing Hanbury Brown-Twiss (HBT) experiments, even at detunings much larger than multiple single-emitter linewidths.

II. RESULTS

A. Device Design

The device studied in this work is pictured in Fig. 1a. Two InAs QDs are coupled to a nanobeam waveguide that supports a single guided mode. The nanobeam is 280 nm wide and 170 nm thick. The positions of the two QDs are marked by white circles. The distance between the QDs is approximately 20 μm —roughly $70\times$ the wavelength of light in the waveguide. This distance is sufficiently large to enable individual Stark tuning of the two emitters. The two QDs can be separately addressed using two driving lasers, and emission is collected from the grating outcoupler at the end of the waveguide.

In this work we use separate Stark tuning of the two QDs to control the detuning between the emitters. To achieve this, the QDs are located in a split diode structure, allowing different voltages to be applied to different sections of the device. The membrane consists of a p-i-n diode with AlGaAs tunnelling barriers to increase the QD tuning range (see Sec. IV). A shallow etch is used to break electrical conductivity through the top p-doped layer of the diode, allowing different voltages to be applied to the separate regions. The positions of this etch are marked in yellow in Fig. 1a, and the red and blue colouring indicates the two electrically isolated regions. The geometry of the shallow etch through the waveguide is optimised using an inverse design technique to minimise loss, an SEM image of the shallow waveguide etch is inset in Fig. 1a. We estimate that the electrical isolation etch results in a $< 1\%$ transmission loss across a broad bandwidth [35].

Relative tuning of the two QDs is shown in Fig. 1b. For this measurement, both QDs are excited using above-band lasers and emission is collected from the outcoupler. The voltage applied to QD1 is held constant at 1.17 V. The voltage applied to QD2 (the red section in Fig. 1a) is tuned, blueshifting the emission from QD2 as the voltage is increased. It can be seen that QD1 is also tuned, due to cross-talk between the two diodes, however QD1 redshifts with increasing voltage. At approximately 1.15 V the two QDs are near-degenerate.

B. Superradiance

The QDs are well approximated as two-level systems, each with a ground state $|g_{1,2}\rangle$, excited state $|e_{1,2}\rangle$, and decay rates $\gamma_{1,2}$. Embedding both QDs in a waveguide allows them to couple effectively to a set of confined one-dimensional modes, which allows for the observation of superradiance. Then, two QDs with similar transition energies form the four-level system shown in Fig. 1c. Optical transitions from the doubly excited state $|e_1, e_2\rangle$ to the ground state $|g_1, g_2\rangle$ occur along the bright single-excitation state $|B\rangle$ with an enhanced rate $\Gamma_D = 2\gamma$ compared to individual decay rate γ , while the dark state $|D\rangle$ has no transition dipole and therefore remains unoccupied. Importantly, both the bright and the dark state are coherent superpositions of the individual QD excited states $|e_1, g_2\rangle$ and $|g_1, e_2\rangle$. For convenience, by absorbing phase factors into the state definition, they can be expressed as the symmetric, $|B\rangle = (|e_1, g_2\rangle + |g_1, e_2\rangle)/\sqrt{2}$, and antisymmetric superposition, $|D\rangle = (|e_1, g_2\rangle - |g_1, e_2\rangle)/\sqrt{2}$. Differences of the QD dipole strengths and imperfections of the waveguide (captured by a waveguide quality factor $\beta < 1$) lead to a reduction of superradiance by changing the transition dipole of the bright and dark states, i.e. to a nonzero dark state decay rate Γ_B in addition to the reduced bright state decay rate $\Gamma_D < 2\gamma$.

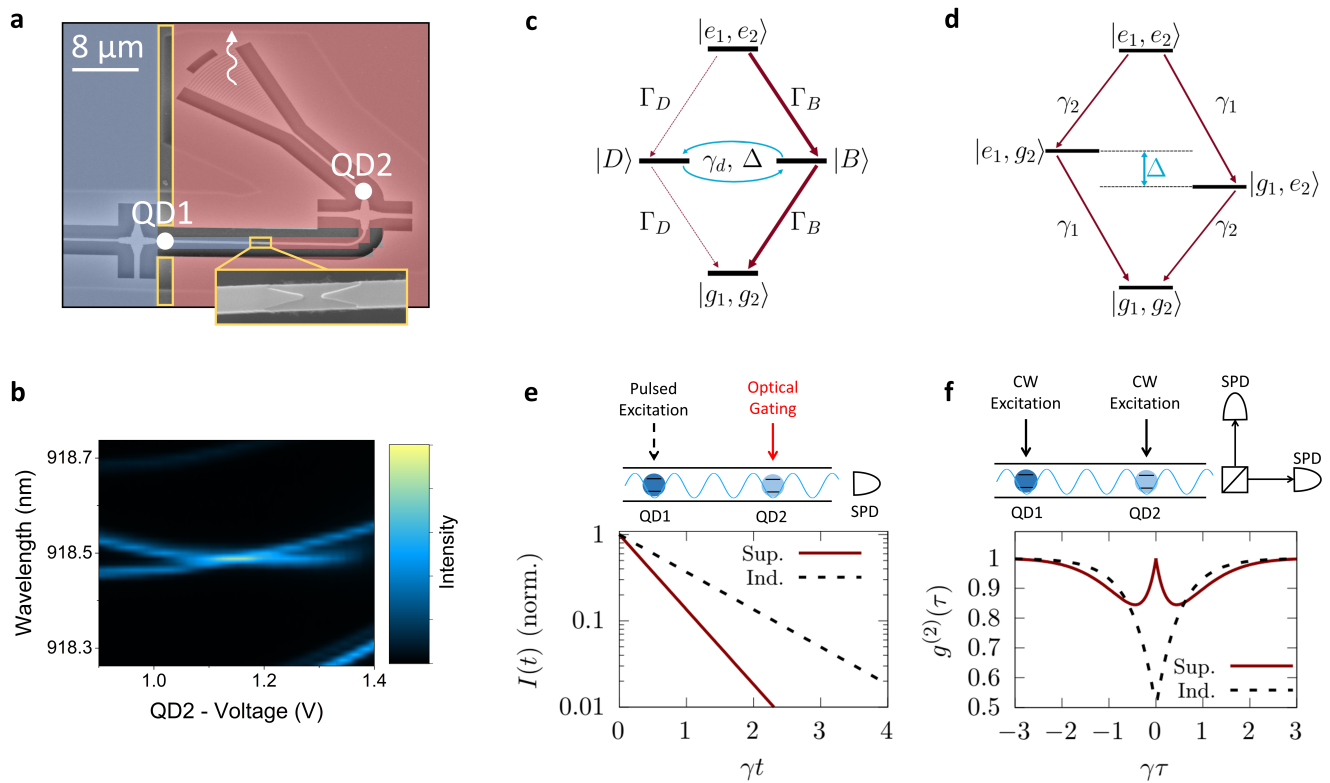


Figure 1. **Independent tuning of QDs and properties of superradiant emission** (a) SEM image of the waveguide device. The positions of the two QDs are marked by white spots. The red and blue colouring marks the area of the two diodes that control the two QDs. Yellow indicates the areas that are etched for electrical isolation. Inset – SEM of the isolation etch in the waveguide. (b) Emission spectrum of the two QDs, measured from the outcoupler of the device, as a function of the voltage applied to QD1 (voltage applied to the blue area in a). (c) Energy level diagram of two resonant waveguide-coupled QDs. (d) Energy level diagram of two independent quantum emitters. (e) Expected intensity decay for an ideal system of two superradiant emitters. (f) Expected autocorrelation function for a pair of superradiant emitters.

Decoherence provides an incoherent transition pathway between the bright and the dark state, further reducing the superradiant enhancement. A non-zero energetic difference between the QD transitions leads to Rabi-like oscillations between dark and bright state. Eventually, with increasing spectral distinguishability, the dynamics are better described by individual QD states, which decay independently of each other (see Fig. 1d). Our theoretical model—including pumping, dephasing, and different properties for the two emitters—is discussed in the supplementary information [35].

Superradiance is expected to manifest itself in two ways. First, intensity measurements of the emitted light, $\langle I(t) \rangle$, reveal an enhancement of the emission rate, with maximum scaling $\propto N^2$ at half inversion [36]. Specifically the emission rate from the bright state $|B\rangle$ scales $\propto N$ (cf. Fig. 1e). This is expected to be the dominant contribution in this experiment, due to the small driving strength. The presence of dephasing and energetic detuning changes this, introducing a bi-exponentiality as the dark state becomes accessible [25, 28].

Performing HBT experiments allows one to access inter-emitter coherences created by the transition from the doubly excited to the ground state via the bright state. In a continuous-wave (CW) excitation setup the corresponding photon coincidence correlations can be expressed as

$$g^2(\tau) = \frac{\langle I(\tau)I(0) \rangle_{SS}}{\langle I(\tau) \rangle_{SS} \langle I(0) \rangle_{SS}}, \quad (1)$$

where the index $\langle \bullet \rangle_{SS}$ indicates the expectation value with respect to the steady state. Then, because the antisymmetric state has a weaker contribution to the emitted intensity, two-photon emission processes are enhanced compared to single photon emission leading to a characteristic anti-dip in the HBT signal around zero time delay. We show this explicitly in Fig. 1f in the case of no decoherence and the individual incoherent pumping rates being equal to the single-emitter decay rates. Additionally, a finite energy difference between the QDs leads to an oscillating phase relationship between the emitters, which manifests as a detuning-dependent beating.

Importantly, the anti-dip in the HBT signal results from relating the emission of a detected photon to a transition from, or into, a correlated emitter state (the bright state). For waveguide-coupled QDs this is naturally the case for photons at the waveguide out-coupler. Therefore, the observation of an anti-dip does not by itself prove superradiance with its associated decay rate enhancement, but only confirms the presence of non-classical correlations in the emission process, which can be observed even for spatially separated, non-superradiant emitters [24, 29, 37, 38].

C. Decay rate enhancement

First, we explore how the radiative decay dynamics are affected by the detuning between the QDs using the excitation scheme shown in Fig. 1e. QD1 is excited with an above-band femtosecond pulse, emission is collected from the outcoupler and correlated with the time of the laser pulses to generate the emission decay curve. The detuning between the QDs is controlled by tuning the voltage applied to QD1. The effect of QD2 on the system is modulated through an optical gating effect [33, 34]. This effect controls the ground state of QD2, such that the near-resonant optical transition can be either active or inactive. The transition is activated using a weak, continuous, above-band laser. This allows us to explore the decay dynamics of a single QD as well as two QDs.

The decay curves with and without optical gating of QD2 at different detunings are presented in Fig. 2(a). From panel (i) It is apparent that the decay is faster when QD2 is active and the QDs are degenerate. This enhanced decay is very sensitive to detuning, and at detunings beyond just 3 μeV the activation of QD2 no longer affects the decay rate.

The decay of a pair of superradiant emitters is not expected to follow a simple exponential decay [28]. Therefore, we choose a metric to assess the decay times in the sample that does not assume mono-exponential decay. In particular, we consider the time $\tau(\epsilon)$ it takes for the intensity to decay from its maximum value I_0 to a threshold of ϵI_0 . In particular, we choose $\epsilon = 1/2, 1/e, 1/10$. We assign errorbars to the extracted decay times by considering the error of extracting the correct value for $\tau(\epsilon)$ for a given data set (see supplementary material [35]).

The detuning dependence of the decay times to these three thresholds is shown in Fig. 2(b). Considering first only the results for the single QD (shown by the darker lines), there is some variation as the QD is tuned. At positive detunings, the decay is slightly faster. We attribute this to a small change in the QD dipole as it is tuned. There is also a slight rise in the decay times for some thresholds around $\Delta = 0$. Note

that at short timescales, these results are impacted by a timing jitter introduced by the non-resonant excitation.

Comparing this to the case where QD2 is active (lighter lines in Fig. 2b), we see that QD2 has little effect on the decay dynamics when the QDs are detuned. At resonance however, we see a significant reduction of about 20% in decay time (cf. Fig. 2b). We attribute this to a superradiant enhancement of the bright state decay rate Γ_B with respect to the single QD decay rate γ_1 . As discussed in Sec. IIB, ideal superradiance would lead to a reduction of decay time by a factor of 2 which is not observed in this sample due to a combination of spectral wandering, a non-unity beta-factor, and the presence of other dephasing sources like, e.g. phonons [35].

For comparison, we develop a theoretical model which considers a finite waveguide quality, decoherence and the non-resonant excitation of QD1 (See supplementary material [35]). As expected, for short to medium time scales our model predicts a drop in the decay time of the system (See Fig. 2c). At long times, the intensity is found to be dominated by the presence of the dark state, leading to an increase in decay time (See Fig. 2c, upper panel). Note that this bi-exponential behaviour of the intensity has been seen in previous experiments [28] but is not visible in our experimental data (cf. Fig. 2b). We attribute this discrepancy to nonradiative decay processes which dominate over the small dark state decay rate. Overall, the lifetime measurements reveal that the emission behaviour of the sample is altered by optically activating QD2. These alterations are significant in the region around zero detuning and lead to a consistent reduction of the observed decay times, indicating a superradiant enhancement.

D. Photon correlations

In addition to the measurements of decay times presented in the previous section, Hanbury Brown-Twiss (HBT) experiments were performed on the same pair of QDs. As outlined in Sec. IIB, and Refs. [24, 38], these allow a direct observation of inter-emitter coherence during the emission process. This way, the presence of inter-emitter coherences can be validated as the source of the drop in radiative lifetime observed in the previous section. For this, both QDs are excited continuously with above-band CW lasers leading to incoherent population of individual QD excitons. Emission is collected from the out-coupler, spectrally filtered to isolate emission from the two QDs, split at a beam splitter, and sent to two single-photon detectors (SPDs). The detuning of the emitters is controlled by tuning the voltage across QD1.

The results of the HBT experiments for different detunings can be seen in Fig. 3. For large spectral

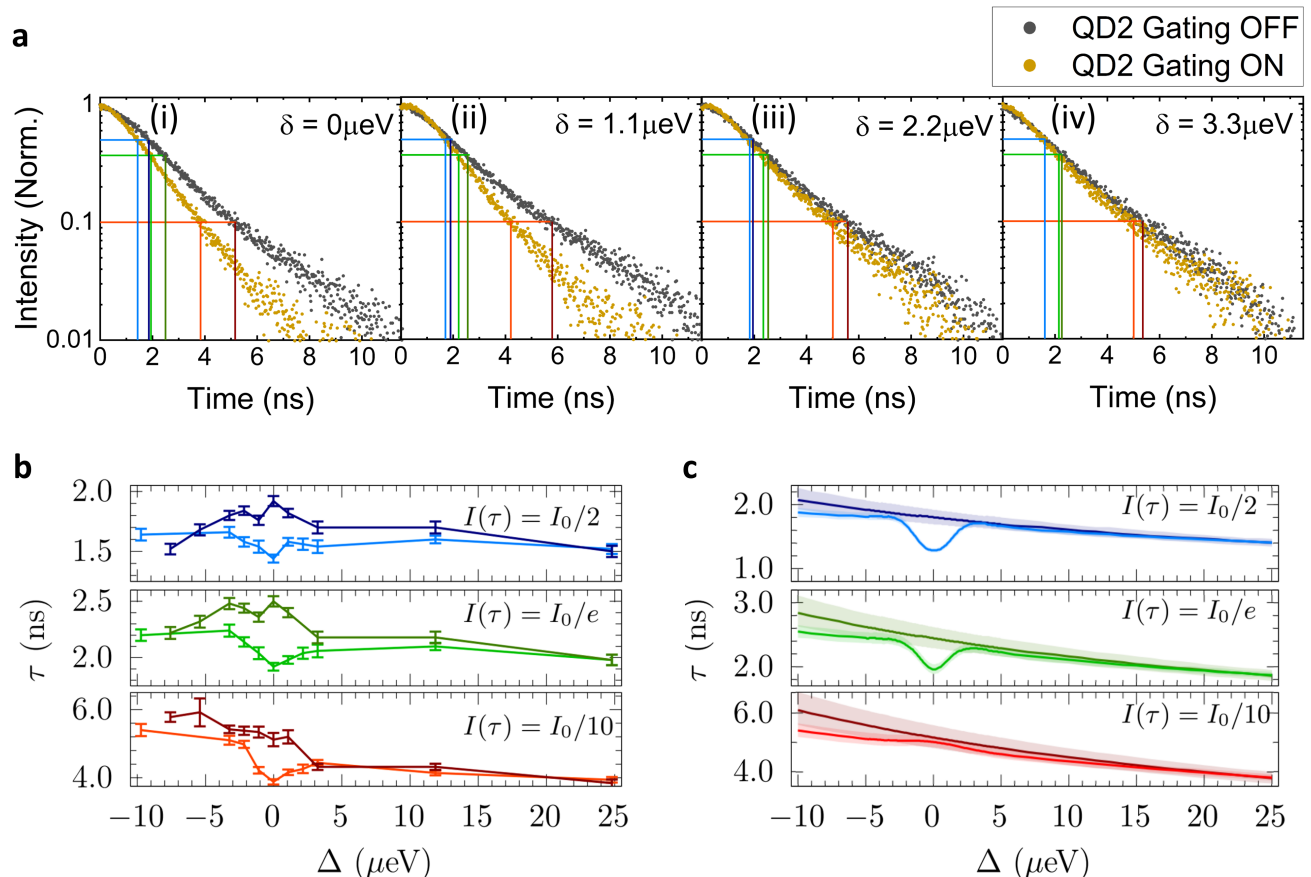


Figure 2. **Enhancement of emitter decay rate.** (a) Comparison of the decay curves of the system with the QDs detuned by (i) $0 \mu\text{eV}$, (ii) $1.1 \mu\text{eV}$, (iii) $2.2 \mu\text{eV}$ and (iv) $3.3 \mu\text{eV}$. Measurements are performed with (yellow) and without (black) optical gating of QD2. Coloured lines indicate where the intensity drops below the thresholds used in (b) and (c). (b) Detuning dependence of the decay rate with (lighter lines) and without (darker lines) gating of QD2. The results are plotted as the time taken for the emission intensity to drop below three threshold values: $I_0/2$ (blue), I_0/e (green) and $I_0/10$ (red). (c) Theoretical prediction of the results in (b). The shaded regions signify uncertainties in the model due to errors in the QD1 lifetime estimation (see main text).

detunings (top panel) the QDs show uncorrelated emission signified by a drop of the two-times correlations to 0.5 at zero time-delay. By contrast, when both QDs are tuned into resonance (bottom panel), an anti-dip approaching unity at zero delay time can be observed, which indicates the presence of inter-emitter coherence after the first photon emission, i.e., the preparation of the bright state by the emission process. At intermediate detunings (centre panels), coherence in the emission process can still be observed at detunings far larger than the single-emitter linewidth, and exceeding the region of rate enhancement that has been observed in Sec. II C (see also Fig. 2c). The detuning between the emitters then manifests itself in a beating behaviour with a beating frequency corresponding exactly to the QD detuning (see Sec. II B). Thus, the transition between the correlated emission at zero detuning and uncorrelated emission can be explained by the beating frequency increasing, until it can no longer be resolved

by the measurement.

Our theoretical model captures the transition between correlated and independent emission and reproduces the height and frequency of the beating with an estimate of spectral wandering of $\sigma = 1.3 \mu\text{eV}$ and a pure dephasing rate of $\gamma_d = (8.0 \pm 1.6) \text{ ns}^{-1}$ which are identical across all HBT experiments. We notice that our theoretical model does not reproduce the small shoulders in the anti-dip of the zero detuning data. The origin of these shoulder may lie in the spectral wandering of the QDs, which is likely to contain jumps that are not captured in the Gaussian line broadening model utilised here.

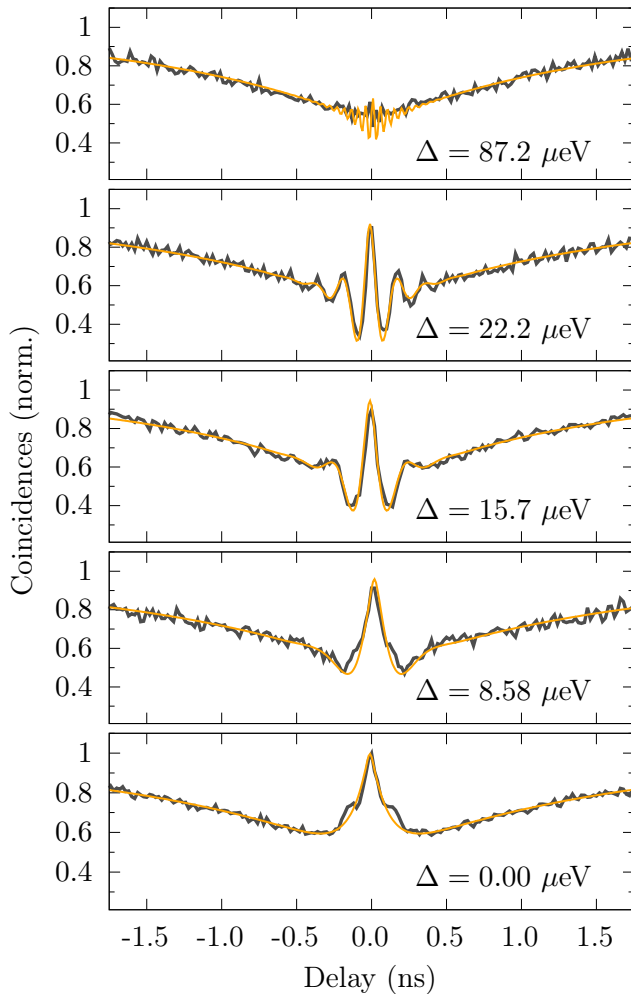


Figure 3. **Photon correlations.** Autocorrelation function of emission collected from the end of the waveguide as a function of emitter-emitter detuning. The yellow lines are theoretical predictions of the measurements.

III. DISCUSSION

In this work we have demonstrated combined Hanbury Brown-Twiss (HBT) and lifetime measurements on a superradiant two quantum dot emitter system. Systematically tuning the quantum dots in and out of resonance, we demonstrated the transition from a superradiant system to fully independent emitters. Most importantly at low to zero detuning we demonstrate a decrease in lifetime of about 20% while at the same time observing an anti-dip around zero delay in the HBT data, which indicates the presence of inter-emitter coherences. At intermediate detunings, we observe a region of cooperative emission without rate enhancement, where inter-emitter correlations can be observed even at detunings of several single-emitter linewidths. Thus, while in the past HBT experiments alone have been presented as evidence for superradiance [26, 27, 31], our

experiments reveal that correlations are still present at very large detunings, where no change in the decay rate is observed, or expected.

We present a gated architecture combined with an optimised waveguide design that enables precise control over the QD detunings while maintaining high coupling efficiencies to the waveguide optical modes. This allowed us to create coherence between distant quantum emitters. This architecture including a fast, reversible, and easily scalable tuning method is therefore an important step towards realising large-scale condensed-matter based quantum networks.

IV. METHODS

A. Nanophotonic devices

The nanophotonic structures are created in a 170 nm GaAs membrane. A layer of QDs is grown at the centre of this membrane using molecular beam epitaxy. The devices are patterned using electron beam lithography, and etched using ICP-RIE. The membrane is grown on top of a 1.1 μm thick sacrificial layer of $\text{Al}_{0.6}\text{Ga}_{0.4}\text{As}$, which is removed using hydrofluoric acid to leave a suspended structure. The top 30 nm of the GaAs membrane is doped with Carbon at a density of $2 \times 10^{19} \text{ cm}^{-3}$. The bottom 30 nm of the membrane is doped with Silicon at a density of $2 \times 10^{18} \text{ cm}^{-3}$. The shallow etch to isolate areas of the device is also defined by electron beam lithography and etched using ICP-RIE to a depth of 40 nm.

B. Theoretical model

In this section we outline our theoretical modelling of superradiant emission from two QDs. More details and derivations of individual terms can be found in Sec. S1 of the Supplementary material [35]. We approximate both QDs as two-level systems such that we can write the Hamiltonian describing both QDs with detuning Δ as

$$H = \frac{\hbar\Delta}{2}(\sigma_1^+\sigma_1^- - \sigma_2^+\sigma_2^-), \quad (2)$$

where $\sigma_{1/2}^+ = |e\rangle\langle g|$ ($\sigma_{1/2}^- = |g\rangle\langle e|$) is the Pauli spin operator acting in the QD1/2 subspace. The mean energy of both QDs can be set to zero without loss of generality. The time evolution of the system density operator can be described by the Lindblad master equation with Lindblad operators $\mathcal{D}[O]\rho = O\rho O^\dagger - (O^\dagger O\rho + \rho O^\dagger O)/2$. We take into account different individual decay rates $\gamma_{1/2}$ for QD1 and QD2 and assume identical dephasing rates γ_d . The finite waveguide quality is captured by the quality factor β , which is equivalent to standard definitions of the β -factor for a single QD [22] (for a derivation, see

supplementary material [35]). Then, the time evolution of the QDs can be written as

$$\begin{aligned} \dot{\rho} = & \frac{1}{i\hbar} [H, \rho] + \beta \mathcal{D}[\Sigma] \rho + (1 - \beta) \mathcal{D}[\sqrt{\gamma_1} \sigma_1^-] \rho \\ & + (1 - \beta) \mathcal{D}[\sqrt{\gamma_2} \sigma_2^-] \rho \\ & + \mathcal{D}[\sqrt{\gamma_d} \sigma_1^+] + \mathcal{D}[\sqrt{\gamma_d} \sigma_2^+] \rho, \end{aligned} \quad (3)$$

where $\Sigma = \sqrt{\gamma_1} \sigma_1^- + \sqrt{\gamma_2} \sigma_2^-$ encapsulates superradiant decay of two emitters with different decay rates and transition frequencies [39]. To describe the spectral wandering present in the sample we perform a Gaussian-weighted average of realisations with different detunings centered around the observed mean detuning as outlined in Sec. S1.3 of the supplementary material [35].

The lifetime data obtained from TCSPC measurements can be described by the intensity $\langle I(t) \rangle \propto \sum_{\mathbf{k}} \langle a_{\mathbf{k}}^\dagger a_{\mathbf{k}} \rangle$, where $a_{\mathbf{k}}^\dagger$ ($a_{\mathbf{k}}$) is the creation (annihilation) operator for the waveguide mode with wave vector \mathbf{k} . Using the Heisenberg equations of motion, waveguide observables can be related to QD degrees of freedom [38]. Thus, we use

$$\langle I(t) \rangle = \langle \Sigma^\dagger \Sigma(t) \rangle / \langle \Sigma^\dagger \Sigma(0) \rangle. \quad (4)$$

As initial state we choose the state of only QD1 being excited, $|e_1, g_2\rangle$, and include the timing jitter induced by the above-band excitation via a convolution of the time evolution with a Gaussian function.

In the HBT experiments, the two-times intensity correlation Eq. (1) is measured. Similarly to the intensity, it can be expressed as

$$g^{(2)}(\tau) = \frac{\langle \Sigma^\dagger(0) \Sigma^\dagger(\tau) \Sigma(\tau) \Sigma(0) \rangle_{\rho_{SS}}}{\langle \Sigma^\dagger(0) \Sigma(0) \rangle_{\rho_{SS}} \langle \Sigma^\dagger(\tau) \Sigma(\tau) \rangle_{\rho_{SS}}}, \quad (5)$$

where the index $\langle \bullet \rangle_{\rho_{SS}}$ indicates the expectation value with respect to the steady state density operator. To account for the CW driving applied in these experiments we add additional terms $\mathcal{D}[\sqrt{\gamma_p} \sigma_1^+] \rho$ and $\mathcal{D}[\sqrt{\gamma_p} \sigma_2^+] \rho$ to the master equation (3).

ACKNOWLEDGEMENTS

Funding: D. H., M.S.S and L.R.W acknowledge support from UK EPSRC (Grant No. EP/V026496/1). M. C. is supported by the Return Program of the State of North Rhine-Westphalia. E.M.G. acknowledges support from UK EPSRC (Grant No. EP/T01377X/1) and from the Leverhulme Trust (RPG-2022-335).

Author contributions: D. H. and L. H performed the experiments. J. W., M. C. and E.M.G. developed the theoretical model. L. H. D. H. and N. M. designed the photonic devices. R. D. fabricated the photonic devices. I. F. and A. V. carried out the growth of the wafer. D. H. and J. W. wrote the manuscript, with contributions from all co-authors. M.S.S. and L.R.W supervised the project.

-
- [1] A. Imamoglu, D. D. Awschalom, G. Burkard, D. P. DiVincenzo, D. Loss, M. Sherwin, and A. Small, Quantum information processing using quantum dot spins and cavity qed, *Phys. Rev. Lett.* **83**, 4204 (1999).
- [2] A. Aspuru-Guzik and P. Walther, Photonic quantum simulators, *Nature Physics* **8**, 285 (2012).
- [3] R. H. Dicke, Coherence in spontaneous radiation processes, *Phys. Rev.* **93**, 99 (1954).
- [4] A. Goban, C.-L. Hung, J. D. Hood, S.-P. Yu, J. A. Muniz, O. Painter, and H. J. Kimble, Superradiance for atoms trapped along a photonic crystal waveguide, *Phys. Rev. Lett.* **115**, 063601 (2015).
- [5] V. V. Temnov and U. Woggon, Photon statistics in the cooperative spontaneous emission, *Opt. Express* **17**, 5774 (2009).
- [6] W. S. Liu and P. Tombesi, Squeezing in a super-radiant state, *Quantum Optics: Journal of the European Optical Society Part B* **3**, 93 (1991).
- [7] D. Pagel, A. Alvermann, and H. Fehske, Nonclassical light from few emitters in a cavity, *Phys. Rev. A* **91**, 043814 (2015).
- [8] J. A. Mlynek, A. A. Abdumalikov, C. Eichler, and A. Wallraff, Observation of dicke superradiance for two artificial atoms in a cavity with high decay rate, *Nature Communications* **5**, 5186 (2014).
- [9] A. González-Tudela and D. Porras, Mesoscopic entanglement induced by spontaneous emission in solid-state quantum optics, *Phys. Rev. Lett.* **110**, 080502 (2013).
- [10] B. Julsgaard and K. Mølmer, Measurement-induced two-qubit entanglement in a bad cavity: Fundamental and practical considerations, *Phys. Rev. A* **85**, 032327 (2012).
- [11] C. Gonzalez-Ballester, A. Gonzalez-Tudela, F. J. Garcia-Vidal, and E. Moreno, Chiral route to spontaneous entanglement generation, *Phys. Rev. B* **92**, 155304 (2015).
- [12] G. Buonaiuto, R. Jones, B. Olmos, and I. Lesanovsky, Dynamical creation and detection of entangled many-body states in a chiral atom chain, *New Journal of Physics* **21**, 113021 (2019).
- [13] A. Politi, J. C. F. Matthews, and J. L. O'Brien, Shor's quantum factoring algorithm on a photonic chip, *Science* **325**, 1221 (2009).
- [14] D. E. Chang, J. S. Douglas, A. González-Tudela, C.-L. Hung, and H. J. Kimble, Colloquium: Quantum matter built from nanoscopic lattices of atoms and photons, *Rev. Mod. Phys.* **90**, 031002 (2018).
- [15] J. Q. Quach, K. E. McGhee, L. Ganzer, D. M. Rouse, B. W. Lovett, E. M. Gauger, J. Keeling, G. Cerullo, D. G.

- Lidzey, and T. Virgili, Superabsorption in an organic microcavity: Toward a quantum battery, *Science Advances* **8**, eabk3160 (2022).
- [16] A. Rastogi, E. Saglamyurek, T. Hrushevskiy, and L. J. LeBlanc, Superradiance-mediated photon storage for broadband quantum memory, *Phys. Rev. Lett.* **129**, 120502 (2022).
- [17] A. A. Kalachev, Quantum memory based on optical subradiance: Optimization of the signal-to-noise ratio, *Bulletin of the Russian Academy of Sciences. Physics* **72**, 691 (2008), copyright - Bulletin of the Russian Academy of Sciences: Physics is a copyright of Springer, 2008; Last updated - 2023-11-21.
- [18] S. Davidson, F. A. Pollock, and E. Gauger, Eliminating radiative losses in long-range exciton transport, *PRX Quantum* **3**, 020354 (2022).
- [19] A. Mottoni, F. Caycedo-Soler, S. F. Huelga, and M. B. Plenio, Design principles for long-range energy transfer at room temperature, *Phys. Rev. X* **11**, 041003 (2021).
- [20] L. Zhai, M. C. Löbl, G. N. Nguyen, J. Ritzmann, A. Javadi, C. Spinnler, A. D. Wieck, A. Ludwig, and R. J. Warburton, Low-noise gas quantum dots for quantum photonics, *Nat. Comms.* **11**, 4745 (2020).
- [21] L. Zhai, G. N. Nguyen, C. Spinnler, J. Ritzmann, M. C. Löbl, A. D. Wieck, A. Ludwig, A. Javadi, and R. J. Warburton, Quantum interference of identical photons from remote gas quantum dots, *Nature Nanotechnology* **17**, 829 (2022).
- [22] P. Lodahl, S. Mahmoodian, and S. Stobbe, Interfacing single photons and single quantum dots with photonic nanostructures, *Reviews of Modern Physics* **87**, 347 (2015).
- [23] M. Arcari, I. Söllner, A. Javadi, S. Lindskov Hansen, S. Mahmoodian, J. Liu, H. Thyrrstrup, E. H. Lee, J. D. Song, S. Stobbe, and P. Lodahl, Near-unity coupling efficiency of a quantum emitter to a photonic crystal waveguide, *Phys. Rev. Lett.* **113**, 093603 (2014).
- [24] J. Wiercinski, E. M. Gauger, and M. Cygorek, Phonon coupling versus pure dephasing in the photon statistics of cooperative emitters, *Physical Review Research* **5**, 013176 (2023), publisher: American Physical Society.
- [25] J. Wiercinski, M. Cygorek, and E. M. Gauger, Role of polaron dressing in superradiant emission dynamics, *Phys. Rev. Res.* **6**, 033231 (2024).
- [26] J.-H. Kim, S. Aghaeimeibodi, C. J. K. Richardson, R. P. Leavitt, and E. Waks, Super-radiant emission from quantum dots in a nanophotonic waveguide, *Nano Letters* **18**, 4734 (2018).
- [27] J. Q. Grim, A. S. Bracker, M. Zalalutdinov, S. G. Carter, A. C. Kozen, M. Kim, C. S. Kim, J. T. Mlack, M. Yakes, B. Lee, and D. Gammon, Scalable in operando strain tuning in nanophotonic waveguides enabling three-quantum-dot superradiance, *Nature Materials* **18**, 963 (2019).
- [28] A. Tiranov, V. Angelopoulou, C. J. van Diepen, B. Schriniski, O. A. D. Sandberg, Y. Wang, L. Midolo, S. Scholz, A. D. Wieck, A. Ludwig, A. S. Sørensen, and P. Lodahl, Collective super- and subradiant dynamics between distant optical quantum emitters, *Science* **379**, 389 (2023).
- [29] Z. X. Koong, M. Cygorek, E. Scerri, T. S. Santana, S. I. Park, J. D. Song, E. M. Gauger, and B. D. Gerardot, Coherence in cooperative photon emission from indistinguishable quantum emitters, *Science Advances* **8**, eabm8171 (2022).
- [30] D. Bhatti, J. von Zanthier, and G. S. Agarwal, Superbunching and Nonclassicality as new Hallmarks of Superradiance, *Scientific Reports* **5**, 17335 (2015).
- [31] A. Sipahigil, R. E. Evans, D. D. Sukachev, M. J. Burek, J. Borregaard, M. K. Bhaskar, C. T. Nguyen, J. L. Pacheco, H. A. Atikian, C. Meuwly, R. M. Camacho, F. Jelezko, E. Bielejec, H. Park, M. Lončar, and M. D. Lukin, An integrated diamond nanophotonics platform for quantum-optical networks, *Science* **354**, 847 (2016).
- [32] X.-L. Chu, C. Papon, N. Bart, A. D. Wieck, A. Ludwig, L. Midolo, N. Rotenberg, and P. Lodahl, Independent electrical control of two quantum dots coupled through a photonic-crystal waveguide, *Phys. Rev. Lett.* **131**, 033606 (2023).
- [33] H. S. Nguyen, G. Sallen, C. Voisin, P. Roussignol, C. Diederichs, and G. Cassabois, Optically gated resonant emission of single quantum dots, *Phys. Rev. Lett.* **108**, 057401 (2012).
- [34] H. S. Nguyen, G. Sallen, M. Abbarchi, R. Ferreira, C. Voisin, P. Roussignol, G. Cassabois, and C. Diederichs, Photoneutralization and slow capture of carriers in quantum dots probed by resonant excitation spectroscopy, *Phys. Rev. B* **87**, 115305 (2013).
- [35] (2023), see Supplementary Material at *inserturl* for a more detailed derivation of the analytical expressions as well as information about the numerically exact calculations.
- [36] M. Gross and S. Haroche, Superradiance: An essay on the theory of collective spontaneous emission, *Physics Reports* **93**, 301 (1982).
- [37] S. Wolf, S. Richter, J. von Zanthier, and F. Schmidt-Kaler, Light of two atoms in free space: Bunching or antibunching?, *Phys. Rev. Lett.* **124**, 063603 (2020).
- [38] M. Cygorek, E. D. Scerri, T. S. Santana, Z. X. Koong, B. D. Gerardot, and E. M. Gauger, Signatures of cooperative emission in photon coincidence: Superradiance versus measurement-induced cooperativity, *Phys. Rev. A* **107**, 023718 (2023).
- [39] G. McCauley, B. Cruikshank, D. I. Bondar, and K. Jacobs, Accurate Lindblad-form master equation for weakly damped quantum systems across all regimes, *npj Quantum Information* **6**, 1 (2020).